

THE EFFECT OF TRAILING-EDGE ELASTICITY ON ITS NOISE RADIATION

Stefan C. Schlanderer¹, Richard D. Sandberg²

¹Aerodynamics and Flight Mechanics Research Group
University of Southampton, SO17 1BJ Southampton, United Kingdom
Email: stefan.schlanderer@soton.ac.uk

²Department of Mechanical Engineering
University of Melbourne, Melbourne VIC 3010, Australia
Email: richard.sandberg@unimelb.edu.au

Abstract

This work aims to investigate the effect of trailing-edge elasticity on trailing-edge noise radiation. To that end a highly accurate and well-validated DNS-code was coupled to a structural solver. The moving body is represented by a novel boundary data immersion method. The effect of trailing-edge elasticity on pressure fluctuations in the far field and the power spectral density are investigated. Our results indicate that depending on the frequency the elastic trailing-edge either acts as a noise amplifier or damper. In-depth spectral analysis of the noise directivity provides insight into the origin of the excess noise observed for the elastic trailing-edge at certain frequencies.

1. Introduction

Trailing-edge (TE) noise is a dominant contributor to noise produced in many engineering applications featuring flows around lifting surfaces such as wings and rotating blades. Recent analytical studies of vibro-acoustic systems by Manela [1], Manela & Huang [2] and Jaworski & Peake [3] concluded that the body motion of an aerofoil or a TE does influence the characteristics of the scattered noise. Depending on the structural parameters and the frequency the noise level can vary significantly. The results of Herr's [4] experiments where brushes were used to replace solid trailing-edges showed that a higher elasticity is beneficial. Despite the fact that the precise role of elasticity was not investigated systematically, the study indicates that an elastic TE can yield noise reductions. This was confirmed by the first DNS of an elastic TE by Schlanderer & Sandberg [5].

Better knowledge of the fluid-structure interaction and its effect on the scattered noise can lead to more silent aerofoil and blade designs. Therefore the present study aims to deepen the understanding in this field by conducting direct numerical simulations (DNS) of flows around elastic trailing-edges. To that end a well validated in-house compressible DNS code is used to directly calculate the near-field hydrodynamics and the far-field sound. Since the numerical method of the structural solver and the method to represent the moving body used in [5] imposed severe timestep restrictions and showed unfavourable behaviour on curvilinear grids, a better suited method was recently developed, implemented and validated in [6].

2. Governing Equations and Numerical Methods

The following two sections introduce the governing equation and numerical methods to solve the fully coupled fluid structure interaction problem and directly calculate the noise radiation from the rigid and elastic TE.

2.1 Fluid

The fluid flow is governed by the fully compressible Navier-Stokes equations. The partial differential equations are discretised with fourth-order accurate standard finite differences. Time stepping is achieved with a five-step fourth-order accurate Runge-Kutta integration. A more detailed description of the code can be found in reference [5].

Besides the accurate calculation of the hydrodynamic and acoustic field, the representation of a moving body in high-fidelity simulations is a severe challenge. To meet this challenge, the boundary data immersion method originally proposed for incompressible flows by Maertens and Weymouth [7] was extended to compressible flows in this work. More details including a validation for aero acoustic applications are presented in [8]. Note that only the first order boundary data immersion method was used in this work.

2.2 Structure

The structure is modelled as a bending beam that is clamped at one side and has a constant cross section with uniform material properties. Furthermore it is assumed that the impact of the fluid on the solid structure is given by the pressure difference between upper and lower side of the plate and leads to small deflections only. The equation of motion for the structure can be modelled by the Euler-Bernoulli beam equation for the deflection w_s and velocity v_s and written as a system of two first order differential equations as

$$\frac{\partial w_s}{\partial t} = v_s \quad (1)$$

$$\frac{\partial w_s}{\partial t} = \frac{1}{\rho_s A} \left(\Delta p - EI \frac{\partial^4 w_s}{\partial s^4} \right), \quad (2)$$

where ρ_s denotes the structural density, A is the cross section of the beam and Δp the line load from the pressure difference. Furthermore EI is the bending rigidity with Young's modulus E and the second moment of inertia of the cross section $I = h^3 d / 12$ with the height h and depth d of the structure. Dimensionless quantities are obtained by nondimensionalizing with the reference fluid density and velocity, or a combination thereof.

The implemented structural solver first calculates the right hand side of equation (2) using the pressure load from the fluid simulation and the spatial derivative of the deflection. The solution is advanced in time by the same fourth-order accurate ultralow storage Runge-Kutta scheme employed in the fluid solver. Additional details about the solver can be found in [6].

4. Computational Setup

The computational domain for this study is shown in Figure 1. It incorporates the TE of a flat plate and its associated wake region. The plate divides two laminar boundary layers that are prescribed at the inflow boundary symmetrically with a displacement thickness of $\delta^* = 2.8 \times 10^{-3}$ using an integrated characteristic boundary condition. The displacement thickness at the TE location is $\delta^* = 9.1 \times 10^{-3}$. In order to create pressure fluctuations that scatter from the TE and drive the structural motion when the elastic TE is considered, a cylindrical vortex generator was inserted upstream of the elastic fraction on the upper side of the flat plate. The strong vortices that will shed from this cylinder are intended to imitate the vortex shedding from the laminar separation bubble of a NACA0012 at angle of attack $\alpha = 5^\circ$ for a chord-based Reynolds number of $Re_c = 5 \times 10^4$ [9]. The free stream Mach number was set to

$M=0.3$ and the global Reynolds Number, based on freestream velocity and unit-length, to $Re=1 \times 10^5$. The timestep for the simulation was $\Delta t=3 \times 10^{-5}$ which results in $CFL \approx 1.07$.

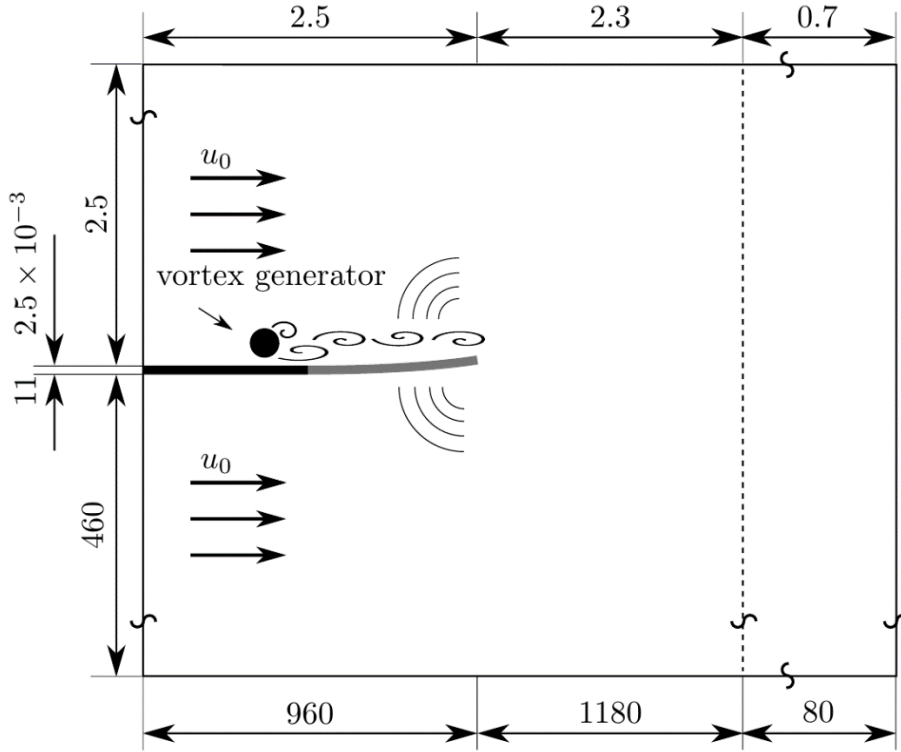


Figure 1. Schematic of the computational setup with the elastic part of the flat plate in grey. The domain is symmetric to the flat plate and the dimensions in the upper half denote lengths and the dimensions in the lower half number of grid points

The computational domain illustrated in Figure 1 is symmetric with respect to the flat plate. The dimensions of this setup are indicated in the upper part of the figure and the number of grid points for each of the sections is shown in the lower part. The aspect ratio of the grid spacing at the TE is $\Delta x/\Delta y=1$. In the wall normal direction the grid spacing was kept equidistant for a height of $h_{eq}=5 \times 10^{-3}$ to make sure that the motion of the elastic plate is adequately resolved. From the TE and the equidistant region, the grid stretches towards the boundaries of the domain. All solid walls i.e. the plate and the cylinder are represented by the boundary-data immersion method (BDIM). At the free stream boundaries above and below the plate and at the outflow non-reflective zonal characteristic boundary conditions[10] were applied to allow acoustic waves to leave the computational domain without spurious reflections. Above and below the plate 10 and at the outflow 120 grid points were used for the zone.

The structural parameters for the simulations employing an elastic TE were chosen such that deflection amplitudes that can be resolved appropriately by the BDIM could be expected. Furthermore, care was taken that the first two natural frequencies of the structure were in the same order of magnitude as the dominant vortex shedding frequency to ensure that the relevant time scales of the structural forcing and its motion match. This is also one of the reasons why only a fraction with the length of $l=0.4$ of the flat plate was considered to be elastic. The Young's modulus of the beam was set to $E=23.04 \times 10^6$ and the structural density to $\rho_s=400$. All of these parameters were nondimensionalized with the reference fluid density and velocity or a combination thereof.

During the simulations with the elastic TE the surface pressure values were evaluated at the beginning of each time step. Then the structural deflection and velocity was calculated by the structural solver for the centre line of the structure on an independent equidistant grid with 60 grid points. After calculating the deflection and velocity of the structure the BDIM was reset at the end of each timestep. This could potentially result in a lag of the pressure information for the structural solver but we found that with the small timestep used for the fluid simulation this effect can be neglected.

5. Results

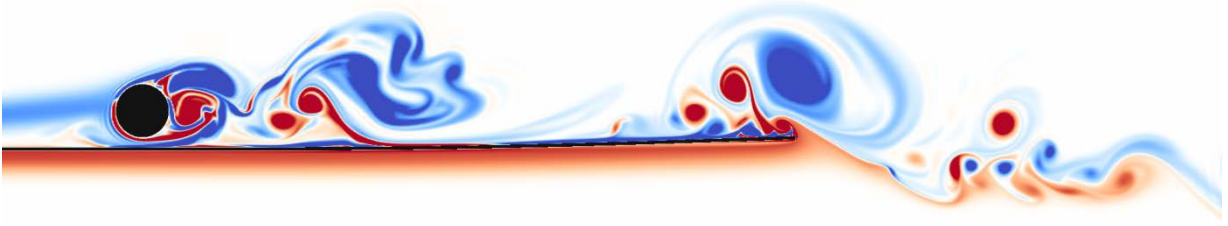


Figure 2. Spanwise vorticity contours for $-70 \leq \omega_z \leq 70$ showing the vortex shedding from the vortex generator and the elastic part of the plate

The spanwise vorticity contours presented in Figure 2 give an initial overview of the hydrodynamic near-field around the elastic fraction of the flat plate and the vortex generator. The vortex generator produces strong, and from visual inspection, non-periodic vortices that are convected over the TE. The pressure fluctuations from these vortices are the incident pressure field for the TE noise mechanism. Therefore the type of noise, i.e. tonal or broadband, will be determined by the characteristics of the shed vortices. In addition, there is a recirculation bubble upstream of the vortex generator which is likely to be caused by its blockage effect on the boundary layer. Furthermore the deflection of the flat plate as a result of the strong pressure disturbances from the vortices can be clearly seen.

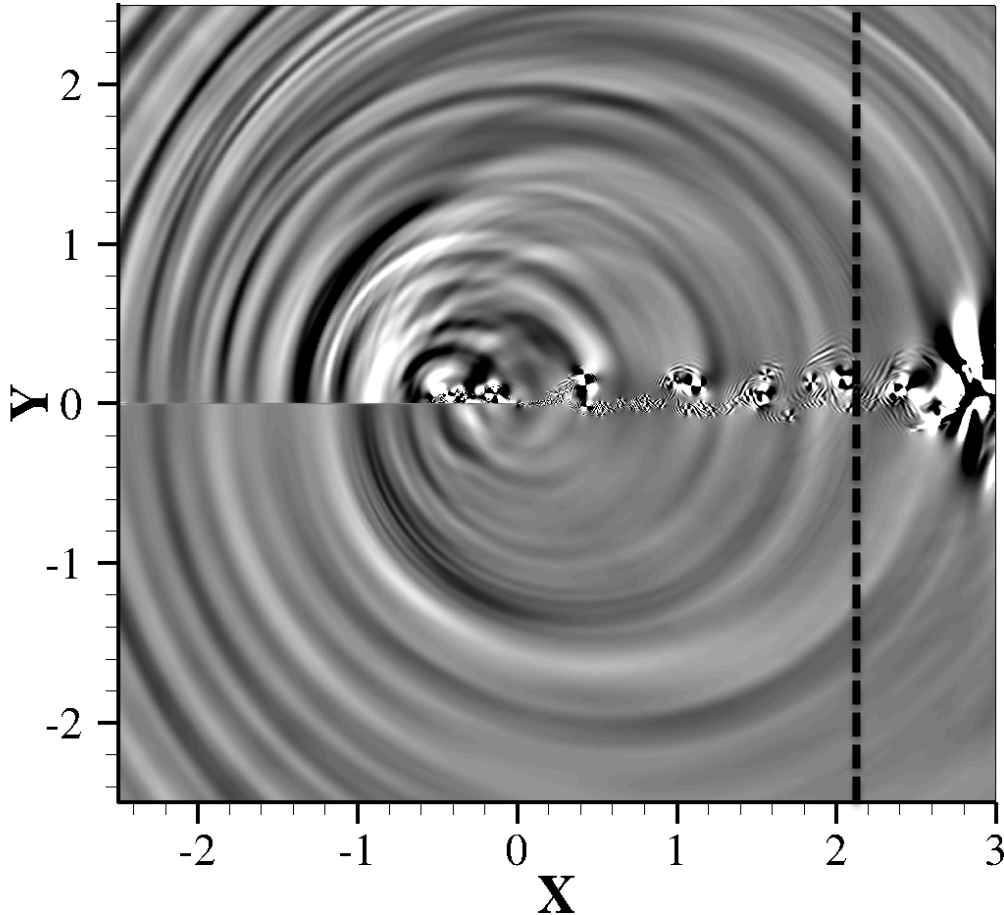


Figure 3. Dilatation contours with levels $[-0.07, 0.07]$ visualizing the acoustic field of the elastic trailing-edge flow

Figure 3 presents the instantaneous dilatation contours obtained from a simulation with an elastic TE to give a first overview of the acoustic field. The TE can be clearly identified as the origin of the acoustic waves. On the upper surface of the plate the noise level seems to be higher, most likely due to excess noise from the vortex generator. In order to isolate the TE noise from this additional noise source as much as possible, all following analysis will focus on the lower side of the plate where applicable. When the contours are examined closely, one can also find quadrupole noise sources in the

wake. According to the acoustic analogy they should radiate less efficiently than the TE noise mechanism for low Mach numbers. This is confirmed by the dilatation field as there are only high wave number and low amplitude acoustic waves radiated from the sources in the wake that decay rapidly. Overall it can be appreciated that there are no reflections from the domain boundaries or from the zone of the characteristic boundary condition at the outflow which starts at $x = 2.3$ and is marked by the dashed line.

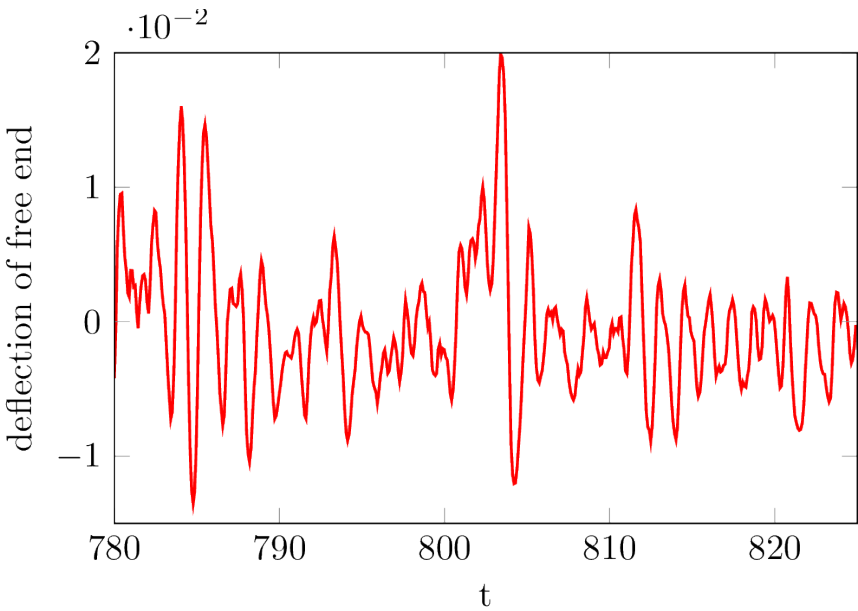


Figure 4. Time history of the deflection of the trailing-edge point

Figure 4 shows an arbitrary sequence in time of the deflection at the TE of the elastic plate. It can be clearly seen that the signal is rather random or a superposition of many different frequencies. This is consistent with the distribution of the shed vortices from the generator plate shown in Figure 2 which generate the loading for the structure.

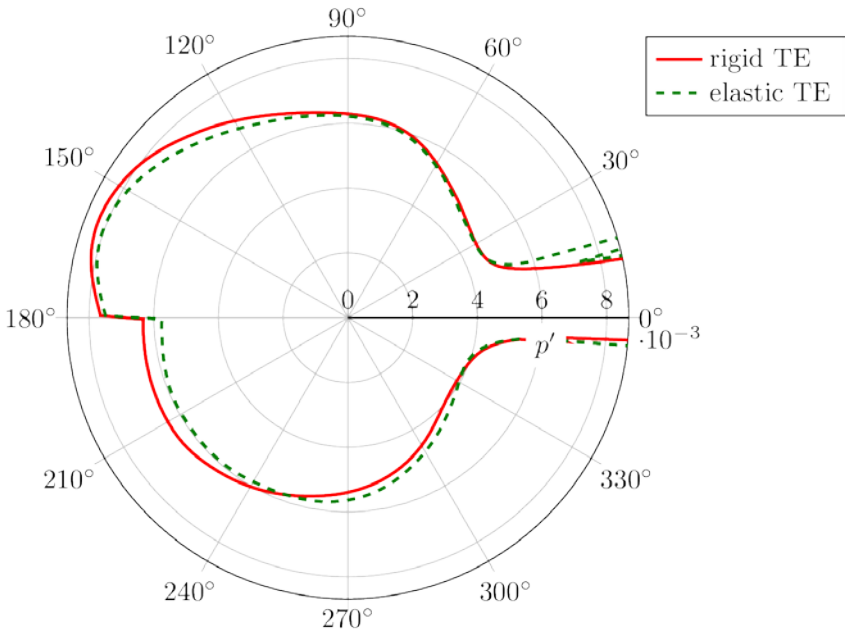


Figure 5. Directivity of the pressure fluctuations at a radial distance of $r = 2.0$ from the trailing-edge comparing rigid and elastic trailing-edge

Figure 5 presents a comparison of the energy of the pressure fluctuation at a radial distance of $r = 2.1$ from the TE between the rigid and the elastic TE. Both cases confirm the initial impression from the instantaneous dilatation contours in Figure 3 that the vortex generator produces additional noise as it is

noisier above the plate. The directivity shows that the elastic TE reduces the scattered noise in the upstream direction. This noise attenuation is more pronounced on the lower side of the plate. However, the directivity pattern in the direction normal to the plate and downstream is not altered, which indicates that the elastic TE has no influence on the noise level of other potential sources in the wake.

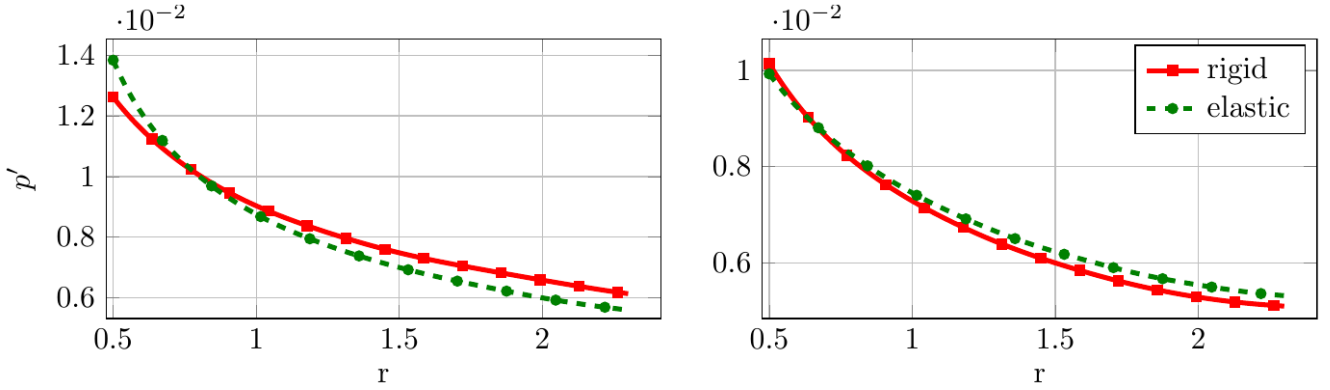


Figure 6. Pressure fluctuation amplitude as a function of radial distance from the TE for an angle of $\theta=185^\circ$ and $\theta=270^\circ$

In order to assess how the noise levels in the two cases vary as a function of radial distance the graphs in Figure 6 compare the energy of the pressure fluctuation amplitude for two selected directions. The first direction that is considered refers to the angle of $\theta=185^\circ$ in the directivity plot and is shown on the left of Figure 6. It shows that the elastic TE is actually noisier than the rigid one in the acoustic near field close to the moving body. With increasing distance from the TE it gets subsequently more silent. This is in contrast to the behavior in the direction normal to the plate with $\theta=270^\circ$ shown on the right of Figure 6. In this direction the elastic TE is more silent in the near field and the noise level becomes higher compared to the rigid case with increasing distance from the TE. The fact that the noise reduction can be found only in a certain direction and starting from a certain distance from the TE indicates that the motion of the elastic TE causes additional noise which decays at a different rate than the pure TE noise.

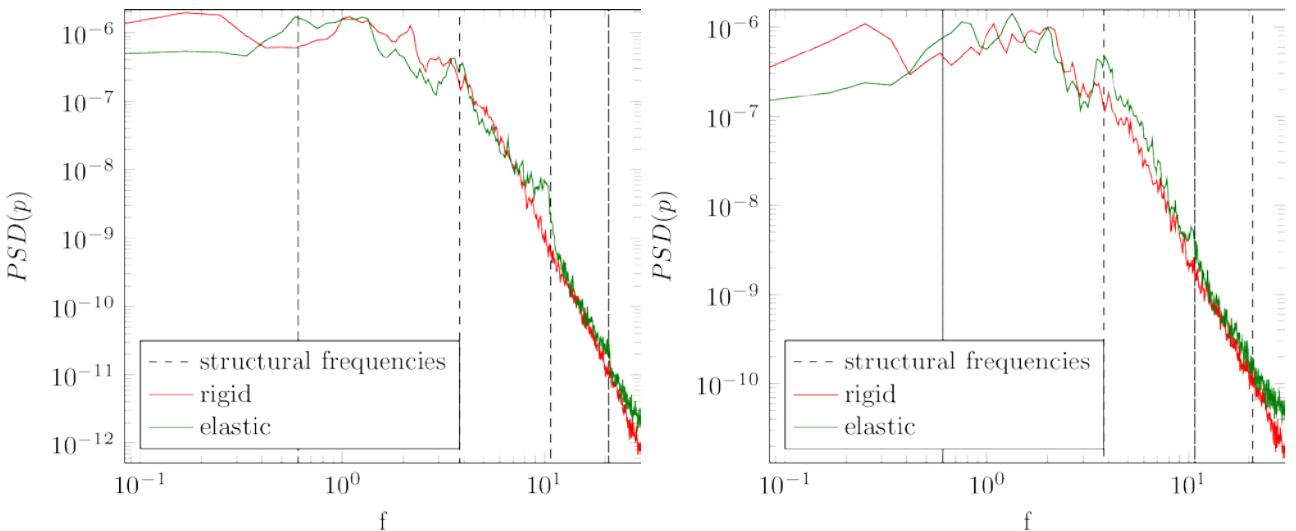


Figure 7. Power Spectral Density of pressure at a radial distance of $r = 2.2$ from the TE and an angle of $\theta = 185^\circ$ and $\theta = 270^\circ$ relating to the directions in the pressure directivity in Figure 5

A spectral analysis of the pressure time history can give further insight into the physical mechanisms that are responsible for the different noise scattering behaviour discovered in the noise directivity. Figure 7 shows the power spectral density of pressure on the lower side of the plate at a radial distance of $r=2.2$ and an angle of $\theta=185^\circ$ on the left and an angle of $\theta=270^\circ$ on the right. Both relate to the directions chosen in Figure 6. The spectra were calculated using Welch's method with 41 Hanning windows and an overlap of 67.5%. Distinct humps can be found in the spectrum of the elastic TE at both locations. The frequencies at which they occur agree well with the the natural frequencies of the

structural motion which are indicated by the dashed lines. They are most pronounced for the first natural frequency at both locations. For the higher natural frequencies the characteristic of the hump differs between the two. Despite of the same energy level it is more pronounced relative to the rest of the spectrum perpendicular to the plate. At the first three eigenfrequencies of the structure the elastic TE is louder than the rigid one, whereas in the low frequency range and between the first and the second natural frequency the elastic TE is less noisy which is in particular true for the upstream direction, i.e. $\theta=185^\circ$.

Apart from the structural frequencies the vortex shedding frequency of the vortex generator can be identified by a distinct peak around a frequency of $f=2$ in the spectrum at the location perpendicular to the plate, i.e. in the right figure.

In order to further investigate the physical characteristics of the noise sources just discussed, a timeseries of pressure in the far field was Fourier transformed to extract the directivity of the spectral power at different frequencies. All together 17 Hanning windows were used with an overlap of 50% using Welch's method. In order to reduce the computational cost of the data capturing and also the postprocessing the analysis focusses on the upstream direction and neglects major parts of the wake.

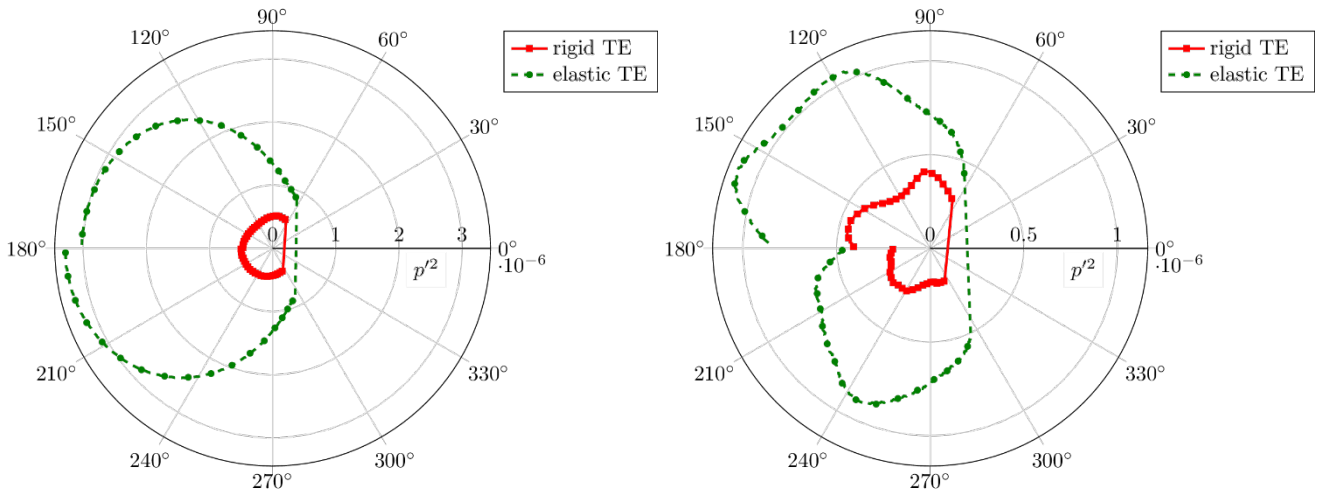


Figure 8. Directivity of spectral power at a radial distance of $r=1.4$ from the TE at the first and second natural frequency of the structural motion, namely $f=0.6$ and $f=3.8$.

The directivity of the first and second natural frequency of the structural vibration is shown in Figure 8. For both frequencies the elastic TE is significantly noisier than the rigid one in all directions where data was recorded. For the first natural frequency a slightly reduced noise level on the upper surface can be observed compared to the lower surface in the elastic case. At this frequency the excess noise is radiating strongest in the upstream direction. The maximum noise level can be found for $\theta=180^\circ$ which is the direction parallel to the plate. This is in contrast to the directivity of the second natural frequency presented in Figure 8 on the right. The maximum of the pure TE noise, i.e. the lower side, is at $\theta \approx 245^\circ$ for the elastic and $\theta \approx 225^\circ$ for the rigid TE. This shows that for this frequency the TE noise is not only amplified but scattered in a different direction.

The spectral power of the vortex shedding frequency $f=2.0$ is considered in Figure 9 on the left. It can be appreciated that the directivity differs significantly when comparing the elastic and the rigid TE cases. On the lower side the noise from the elastic TE is predominantly radiated downstream or perpendicular to the plate and shows higher noise levels than the rigid TE. This behaviour is reversed in the upstream direction where the amplitude of the elastic TE case levels off faster compared to the rigid one. Above the plate the elastic TE features an additional lobe in the upstream direction that is exceeding the spectral power levels of the rigid TE significantly. It can be speculated that this additional lobe is due to an interaction of the excess noise at the natural frequencies of the structural motion and the vortex shedding triggering a stronger noise radiation from the cylinder. This is consistent with the small noise reduction in the upstream direction above the plate observed in the integral noise directivity in Figure 5.

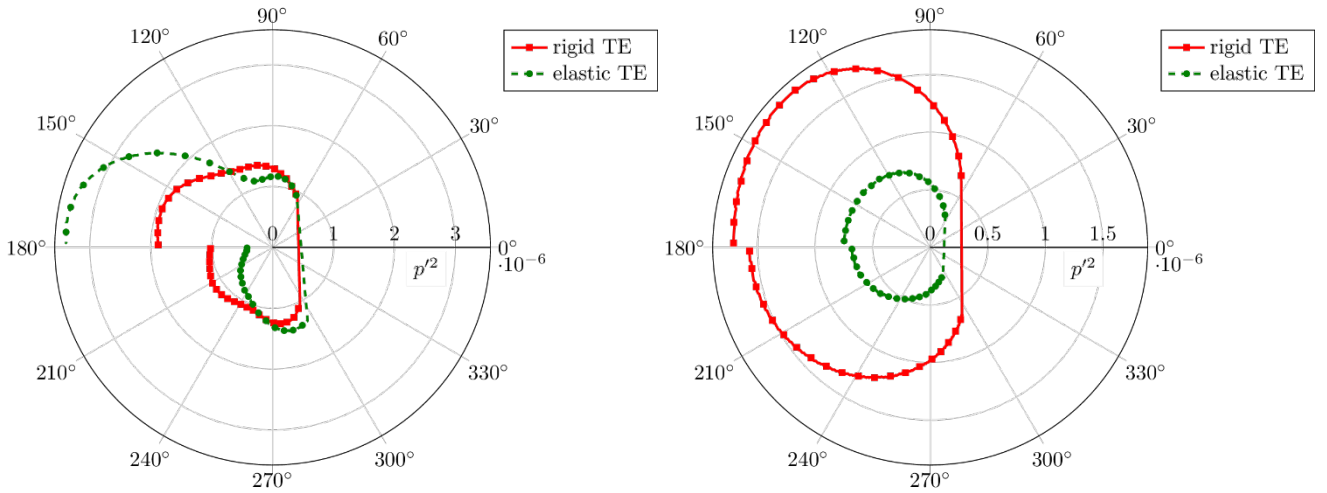


Figure 9. Directivity of spectral power at a radial distance of $r = 1.4$ from the TE at a frequency of $f=2.0$ and $f=0.2$.

In Figure 9 on the right a frequency in the very low frequency range was chosen that showed a significant noise reduction for the elastic TE. In both cases the noise scattering is strongest in the upstream direction. It can be observed that in this case the noise reduction seems to be independent of the direction. Combined with the earlier findings this indicates that the directivity of the noise reduction for the elastic TE is predominantly caused by the directional excess noise from the elastic TE.

5. Conclusions

This paper presents the results from direct numerical simulations of the noise scattering from an elastic TE and compares them to results from simulations with a rigid TE. The motion of the elastic TE causes excess noise that decays at a different rate than the pure TE noise in the rigid case. The excess noise occurs in frequency ranges close to the natural frequencies of the structure. For the frequency ranges not coinciding with the natural frequencies the elastic TE yields a noise reduction. Overall, this reduction outweighs the excess noise and leads to overall total noise reduction using an elastic TE. Spectral analysis of the sound directivity indicates that the noise radiation from the vortex generator is stronger for an elastic TE. Furthermore the excess noise close to the natural frequencies of the structure is at least partly scattered in a different direction than the pure TE noise.

Acknowledgements

The first author gratefully acknowledges the studentship for his PhD funded by the Faculty of Engineering and the Environment of the University of Southampton. Furthermore the computational time on the national supercomputing facility ARCHER provided through the UK Turbulence Consortium under EPSRC Grant EP/L000261/1 is acknowledged.

References

- [1] A. Manela, "Sound generated by a vortex convected past an elastic sheet", *Journal of Sound and Vibration*, **330**, 416-430, (2011).
- [2] A. Manela, L. Huang, "Point vortex model for prediction of sound generated by a wing with flap interacting with a passing vortex", *The Journal of the Acoustical Society of America*, **133**, 1934-1944, (2013).
- [3] J.W. Jaworski, N. Peake, "Aerodynamic noise from a poroelastic edge with implications for the silent flight of owls", *Journal of Fluid Mechanics*, **723**, 456-479, (2013).
- [4] M. Herr, "Design criteria for low-noise trailing-edges", in, *AIAA Paper 2007-3470*.

- [5] S.C. Schlanderer, R.D. Sandberg, "DNS of a Compliant Trailing Edge Flow", *AIAA Paper* 2013-2013, (2013).
- [6] S.C. Schlanderer, R.D. Sandberg, "DNS of an Airfoil at Angle of Attack with an Elastic Trailing-Edge Extension", *19th Australasian Fluid Mechanics Conference*, (2014).
- [7] A.P. Maertens, G.D. Weymouth, "Accurate Cartesian-grid simulations of near-body flows at intermediate Reynolds numbers", *Computer Methods in Applied Mechanics and Engineering*, (2014).
- [8] S.C. Schlanderer, R.D. Sandberg, "Boundary Data Immersion Method for DNS of aero-vibro-acoustic systems", in: *DLES - Direct and Large Eddy Simulations*, ERCOFTAC, 2015.
- [9] L.E. Jones, R.D. Sandberg, N.D. Sandham, "Direct numerical simulations of forced and unforced separation bubbles on an airfoil at incidence", *Journal of Fluid Mechanics*, **602**, 175-207, (2008).
- [10] R.D. Sandberg, N.D. Sandham, "Nonreflecting zonal characteristic boundary condition for direct numerical simulation of aerodynamic sound", *AIAA Journal*, **44**, 402-405, (2006).